Modeling Snow-Cover Heterogeneity over Complex Arctic Terrain for Regional and Global Climate Models*

STEPHEN J. DÉRY

Lamont-Doherty Earth Observatory, Columbia University, Palisades, New York

WADE T. CROW

Hydrology and Remote Sensing Laboratory, USDA ARS, Beltsville, Maryland, and Department of Civil and Environmental Engineering, Princeton University, Princeton, New Jersey

MARC STIEGLITZ

Lamont-Doherty Earth Observatory, Columbia University, Palisades, New York

ERIC F. WOOD

Department of Civil and Environmental Engineering, Princeton University, Princeton, New Jersey

(Manuscript received 25 November 2002, in final form 12 September 2003)

ABSTRACT

The small-scale (10 to 100 m) and local-scale (100 m to 10 km) effects of topography (elevation, slope, and aspect) and snow redistribution by wind on the evolution of the snowmelt are investigated. The chosen study area is the 142 km^2 Upper Kuparuk River basin located on the North Slope of Alaska. Two land surface models (LSMs) designed for regional and global climate studies apply different techniques to resolve these additional processes and features and their effects on snowmelt. One model uses a distributed approach to simulate explicitly the effects of topography on snowmelt at a 131-m resolution across the entire Upper Kuparuk watershed. By contrast, the other LSM employs a simple parameterization to implicitly resolve the effects of wind-blown snow on the hydrology of the Upper Kuparuk basin. In both cases, the incorporation of these local- and small-scale features within the LSMs leads to significant heterogeneity in the 1997 end-of-winter spatial distribution of snow cover in the Upper Kuparuk watershed. It is shown that the consideration of subgrid-scale snow-cover heterogeneity over complex Arctic terrain provides a better representation of the end-of-winter snow water equivalent, an improved simulation of the timing and amount of water discharge of the Upper Kuparuk River, and an alteration of other surface energy and water budget components.

1. Introduction

Snow seasonally covers up to 40% of the Northern Hemisphere landmass (Hall 1988) and constitutes the most prominent transient feature across continental surfaces (Cohen and Rind 1991). With its elevated albedo and high thermal emissivity, a snow cover leads to a suppression of near-surface air temperatures (Ellis and Leathers 1998). The low thermal conductivity of snow insulates well the underlying ground from the relatively cold atmosphere (Goodrich 1982; Osterkamp and Romanovsky 1996; Stieglitz et al. 2003a). Through surface and blowing sublimation processes, a snow cover constitutes a sink of energy near the surface while providing a source of atmospheric moisture (Déry et al. 1998). During the spring transition period, snow retained in this temporary reservoir is quickly released, yielding high runoff rates that contribute as much as 80% of the yearly discharge rates of some Arctic streams and rivers (McNamara et al. 1998).

The current generation of land surface models (LSMs) designed for climate studies typically has only a basic representation of snow processes (e.g., Slater et al. 2001). One assumption often invoked by climate modelers is that the snow cover retains spatial uniformity within a model grid cell. In many regions such as the North Slope of Alaska, however, the snow cover exhibits considerable spatial heterogeneity (Fig. 1). This situation arises because of the topographic control of precipitation, radiation, and temperature, and the redis-

* Lamont-Doherty Earth Observatory Contribution Number 6542.

Corresponding author address: Stephen J. Déry, Lamont-Doherty Earth Observatory, Columbia University, Palisades, NY 10964-8000. E-mail: dery@1deo.columbia.edu

FIG. 1. Photograph showing the end-of-winter snow-cover distribution at Toolik Lake and the Upper Kuparuk River basin, with the Brooks Range in the background. The photo was taken on 28 May 1996 facing southward by G. W. Kling, University of Michigan.

tribution of snow by wind. Therefore, the assumption of a spatially homogeneous snow cover may lead to degradation in simulations of the surface energy budget, snowmelt, and runoff.

In this paper, we investigate the evolution of snowmelt over complex Arctic terrain as simulated by two LSMs developed for climate studies. In their current states, these LSMs neglect spatial heterogeneity in the snow cover within a model grid cell. We therefore explore separately the impact that topography (i.e., elevation, slope, and aspect) and wind redistribution have on reducing model uncertainties for simulations of the snowmelt period in the Arctic climate system. The objectives of this study are 1) to identify the critical small-scale snow processes that need to be incorporated in climate simulations of the Arctic ecosystem and 2) to explore methods that better represent these processes in regional and global climate models.

The outline of the paper is as follows: In section 2, we provide some background information on past strategies employed to model snow-cover formation and ablation processes. Subsequently, we describe in section 3 an Alaskan watershed that forms the test bed of our study. This is followed in section 4 by a description of the forcing and validation datasets used in this work. Section 5 presents a summary of two LSMs that are applied in this study. Section 6 presents results from a series of numerical experiments using the LSMs after their adaptation to the Arctic environment. Last, in section 7, we summarize our findings, discuss the implications of our work, and provide direction for future work.

2. Background

Spatial variability in snow cover is found on regional (10 to 1000 km), local (100 m to 10 km), and small (10 to 100 m) scales (McKay and Gray 1981; Pomeroy and Gray 1995). Atmospheric processes and patterns that govern storm tracks and the formation of solid precipitation determine the spatial distribution of snow on a regional scale (Stewart et al. 1998). Altitudinal control over precipitation type and intensity (by enhanced orographic lifting), in addition to ambient air temperatures, contribute to regional and local nonuniformity in the snow cover. At local scales, the elevation, slope, and aspect regulate the amount of incoming radiation available for melt. Snow redistribution during high-wind events further enhances the heterogeneous aspect of the snow cover at local to small scales. The presence of trees and other vegetation also influences the small-scale distribution of snow depth (McKay and Gray 1981; Woo and Steer 1986).

Because of numerical efficiency requirements and other considerations, the current generation of LSMs applied in climate studies generally offers reduced levels of complexity to represent local- and small-scale snow processes at regional scales (e.g., Slater et al. 2001). One approach used by Walland and Simmonds (1996) is a scheme relating snow-cover heterogeneity to sub-

grid-scale variations in topography and to the surface vegetation within a general circulation model (GCM) grid cell. Another, used by Bowling et al. (2000), is the partitioning of river basins into elevation bands to resolve the effects of altitude on snow-cover formation and ablation processes. Others have related the snow water equivalent to the snow areal fraction to circumvent the explicit simulation of small-scale snow processes (Anderson 1973; Roesch et al. 2001; Slater et al. 2001). Déry and Yau (2002) considered wind redistribution by applying parameterizations for the transport and sublimation of blowing snow in a regional-scale study of the surface water balance. They determined that computing the divergence of snow mass transport over large areas yields underestimates of the small-scale snow heterogeneity found in nature.

For local- and small-scale numerical studies, computational efficiency becomes less of a concern such that snow processes are often modeled in a distributed fashion. In this situation, the spatial variability is restricted only by the grid spacing used in the simulations. For instance, Blöschl et al. (1991) showed considerable success in a process-based modeling study of the snow cover at a 25-m resolution for a 9.4-km^2 alpine watershed. Their distributed approach accounted for topographic variations in solar radiation and their effects on snowmelt. Several distributed models have recently been developed to explicitly resolve the redistribution of snow by wind at various locations (e.g., Liston and Sturm 1998, 2002; Essery et al. 1999; Déry and Yau 1999a, 2001a,b; Xiao et al. 2000; Prasad et al. 2001). Based on snow depth observations, Luce et al. (1998, 1999) defined snowdrift factors by which gridpoint solid precipitation was multiplied to represent blowing snow in the 0.26-km^2 Upper Sheep Creek watershed in Idaho. Hartmann et al. (1999) applied a similar snow mass redistribution scheme by taking grid points in highlands (lowlands) as mass accumulation (erosion) zones in their study of a 6.6-km^2 watershed in the Rocky Mountains. Others have sought to relate terrain type with the spatial variations in snow depth (Woo and Marsh 1978; Winstral et al. 2002).

We present steps that lead to the inclusion of local- and small-scale variations in snow cover as a result of various physical processes in two LSMs adapted to simulate the Arctic climate system. The first is the catchment-based land surface model (CLSM) of Koster et al. (2000) and Ducharne et al. (2000) that has been developed specifically for inclusion within the National Aeronautics and Space Administration (NASA) Seasonal-to-Interannual Prediction Project (NSIPP) GCM. The second model is a recent version of the TOPMODEL-based Land–Atmosphere Transfer Scheme (TOPLATS; Pauwels and Wood 1999a,b) that has been developed and tested with its focus on small-scale process studies. Both the CLSM and TOPLATS contain snow modules that are modified in this work to account for local- and small-scale snow heterogeneity (see section 5). To demonstrate the effectiveness of our proposed modifications to these LSMs, we examine the Upper Kuparuk watershed located on the Arctic tundra north of the Brooks Range of Alaska. As illustrated in Fig. 1, the snow cover of this basin exhibits considerable local- to small-scale variability as a result of its range in elevations, slopes, and aspects, as well as the frequent occurrence of blowing snow in the area (Zhang et al. 2000). The Upper Kuparuk is also the site of a number of ongoing field studies on the Arctic tundra (e.g., Kane et al. 2002), and this region has been the test bed for modeling studies of North Slope hydrometeorological and biogeochemical processes (Stieglitz et al. 1999, 2000, 2003b; Zhang et al. 2000).

3. The Upper Kuparuk watershed

The Upper Kuparuk River flows northward from the foothills of the Brooks Range and eventually becomes the Kuparuk River that discharges into the Arctic Ocean near Prudhoe Bay, Alaska. The Upper Kuparuk watershed is centered near 69.63°N, 149.40°W at an average altitude of 967 m and covers 142 km^2 in area (McNamara et al. 1998). Its vegetation consists generally of tussock tundra, with shrubs, wet sedge, dry heath, and lichens also permeating its surface (Walker and Walker 1996). The predominant soils in the Upper Kuparuk watershed are composed of an organic peat in the first 15–20 cm, underlain by silt and glacial till (Hinzman et al. 1991). Continuous permafrost with depths reaching 600 m controls the basin's subsurface hydrology to a large extent (Osterkamp and Payne 1981; McNamara et al. 1998).

The climate of the Upper Kuparuk is dominated by a lengthy snow-cover season extending from September to early June. Typically, snowmelt provides one-third of the river's annual runoff (Kane et al. 2000). This percentage is less than other rivers on the Arctic tundra since the Upper Kuparuk is more susceptible to orographic rainstorms during the warm season than other Arctic watersheds under study. Snowfall accumulation is relatively low, with a typical value of 130-mm snow water equivalent (swe) in any given year (Zhang et al. 1996; McNamara et al. 1998). Solid precipitation accounts for 33% to 40% of the annual precipitation input into the catchment and may occur at any time of the year (Kane et al. 2000). The mean annual air temperature for the Upper Kuparuk is in the vicinity of −8°C (Zhang et al. 1996).

4. Datasets

The Upper Kuparuk is selected as our test bed since unlike most other northern catchments, it has been the subject of intense field experiments. In this context, two main field sites, Imnavait Creek and Toolik Lake, have been fully instrumented such that a comprehensive meteorological record for the past 15 yr exists. Imnavait

TABLE 1. List of the meteorological stations in the vicinity of the Upper Kuparuk River basin, their abbreviations, geographical coordinates, elevation, and associated meteorological fields (even if only partially available throughout 1996 and 1997). The measurements of surface air temperature (T), relative humidity with respect to water (RH), wind speed (U), surface atmospheric pressure (P_s), incoming shortwave ($K^{\downarrow}$) and longwave ($L^{\downarrow}$) radiation, snowfall (S), and precipitation rate (P) are listed where available. The data are taken from Kane et al. (2002), Kane and Hinzman (2002), and the Arctic LTER database (http://ecosystems.mbl.edu/arc/).

Station	Abbreviation	Lat (°N)	Lon (°W)	Elev (m)	Available fields
Betty Pingo	BM	70.27	148.88	12	P, RH, T, U
East Headwater	EH	68.57	149.30	909	P, T, U
Franklin Bluffs	FB	69.83	148.60	78	$K^{\downarrow}$, $L^{\downarrow}$, RH T, U
Green Cabin Lake	GL	68.53	149.22	975	P, T, U
Imnavait Creek	IA	68.62	149.28	910	$K^{\downarrow}$, $L^{\downarrow}$, P, P_s, RH, S, T, U
North Headwater	NH	68.60	149.42	944	P, T, U
Sagwon	SH	69.42	148.75	299	$K^{\downarrow}$, $L^{\downarrow}$, P, RH, T, U
Toolik Lake	TK	68.63	149.60	900	$K^{\downarrow}$, P, P_s, RH, T, U
Upper Headwater	UH	68.52	149.33	1003	P, T, U
Upper Kuparuk	UK	68.63	149.40	774	P, RH, T, U
West Dock	WD	70.37	148.55	8	$K^{\downarrow}$, $L^{\downarrow}$, P, RH, T, U
West Headwater	WH	68.55	149.40	1018	P, T, U
West Kuparuk	WK	69.42	150.33	160	$K^{\downarrow}$, $L^{\downarrow}$, P, P_s, RH, T, U

Creek is situated just to the northeast of the Upper Kuparuk watershed whereas the Toolik Lake Long-Term Ecological Research (LTER) site is slightly to its northwest. A dozen or so meteorological stations scattered across the region supplement the measurements carried on at Imnavait Creek and Toolik Lake. The observations collected at these sites have undergone extensive quality control and validation (Kane et al. 2002). They have also been applied in numerous studies of Arctic hydrology (e.g., Hinzman and Kane 1991, 1992; Kane et al. 1991; Stieglitz et al. 1999, 2000, 2003b; Zhang et al. 2000).

a. Meteorological observations

To force the numerical models, meteorological data from 13 sites located in the vicinity of the Upper Kuparuk basin are utilized (Table 1). The period chosen for this study begins on 1 January 1996 and terminates on 31 December 1997, with emphasis on the 1997 spring melt period. This period is chosen to maximize the number of stations with available forcing data in the watershed in addition to the typical climate conditions encountered at this time (see discussion below). The standard meteorological variables of the near-surface air temperature $T(K)$, the relative humidity RH(%) and wind speed $U(\text{m s}^{-1})$ are available at nearly all stations. Other required meteorological fields for the numerical simulations are the surface atmospheric pressure P_s(hPa), the precipitation rate $P(\text{mm h}^{-1})$, the incoming solar radiation $K^{\downarrow}(\text{W m}^{-2})$ and the incoming longwave radiation $L^{\downarrow}(\text{W m}^{-2})$. All of these fields are averaged based on a least squares weighting scheme from the measurement sites to the geographical center of the Upper Kuparuk basin. This approach yields a nearly continuous time series in each of the required forcing variables at hourly intervals while substantially reducing the gaps during which data were unavailable from certain locations. It also provides a dataset with good spatial distribution, although some of the higher elevations in the Upper Kuparuk basin remain underrepresented. Daily snowfall data from the Imnavait Creek Wyoming snow gauge, operated by the Natural Resources Conservation Service (NRCS), are added to supplement liquid precipitation measurements from the tipping rain buckets. We assume that all snow fell equally during the day of measurement such that the daily values are divided by 24 to provide hourly wintertime precipitation data. Note that snowfall rates are enhanced by 25% at a constant rate for all wind speeds[1] to correct for undercatch and wetting losses, as well as the omission of trace events by the Wyoming snow gauge (Yang et al. 2000).

Following the interpolation of these fields onto the Upper Kuparuk basin, some significant gaps remain in the values of $L^{\downarrow}$. We therefore estimate longwave radiation as follows (Jones 1992):

$$L^{\downarrow} = \sigma(T - 20)^4, \tag{1}$$

where $\sigma(=5.678 \times 10^{-8}\ \text{W m}^{-2}\ \text{K}^{-4})$ is the Stefan–Boltzman constant. This simple formulation is used since the observational database does not contain cloud cover or upper-level humidity measurements as is often required in other parameterizations of $L^{\downarrow}$. Shorter temporal gaps ($<$24 h) in P_s are eliminated by simple linear interpolation of this field.

Figure 2 presents the evolution of all the meteorological fields in the Upper Kuparuk basin during May and June of 1997. A summary of the annual climatology for 1996 and 1997 is also provided in Table 2. This demonstrates that the annual mean temperature for 1996–97 did not deviate much from the values reported by Zhang et al. (1996) for the Toolik Lake area. Precipitation totals are near the 1993–95 average of 388

[1] Investigation on the impact of a wind-dependent gauge correction factor generated little difference in the end-of-winter swe for the year of interest.

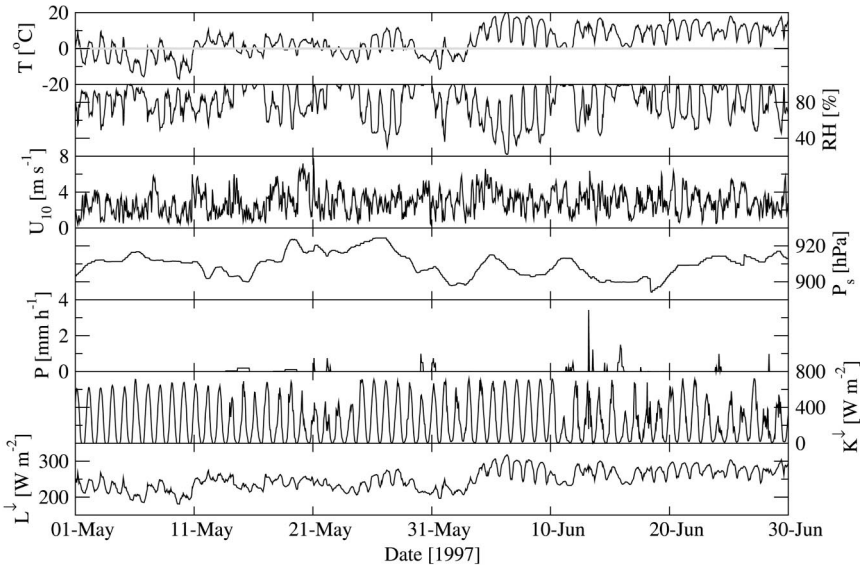

FIG. 2. The observed values of surface air temperature (T), relative humidity with respect to water (RH), 10-m wind speed (U_{10}), surface atmospheric pressure (P_s), precipitation rate (P), and incoming solar ($K^{\downarrow}$) and longwave ($L^{\downarrow}$) radiation for the Upper Kuparuk River basin at hourly intervals during May and Jun 1997. The data are taken from Kane et al. (2002), Kane and Hinzman (2002), and the Arctic LTER database (http://ecosystems.mbl.edu/arc/).

mm documented by McNamara et al. (1998) for the Upper Kuparuk basin, with snowfall accounting for nearly 40% of the annual precipitation. Also, the mean relative humidity with respect to ice RH_i (percent), calculated only in subfreezing conditions, is on average 88% during these 2 yr. This is considerably less than the ice saturation point and suggests that the hygrometers operating at these locations are not as susceptible to icing as those at Canadian climate autostations (Déry and Stieglitz 2002). Finally, the prevailing winds in the Upper Kuparuk are from the southern quadrant.

TABLE 2. Values of the mean annual surface air temperature (T), relative humidity with respect to water (RH), relative humidity with respect to ice (RH_i), 10-m wind speed (U_{10}), 10-m wind direction (ϕ), surface atmospheric pressure (P_s), and incoming shortwave ($K^{\downarrow}$) and longwave ($L^{\downarrow}$) radiation, as well as the total yearly precipitation (P), snowfall (S), and river runoff (R) for the Upper Kuparuk River basin in 1996 and 1997. Note that values of RH_i are computed only when $T < 0$°C and that southerly winds are given by $\phi = 180$°.

Variable	1996	1997
T (°C)	−9.5	−8.8
RH (%)	74.7	75.3
RH_i (%)	87.5	89.0
U_{10} (m s^{-1})	3.2	2.9
ϕ (°)	186.0	183.0
P_s (hPa)	908.0	909.0
$K^{\downarrow}$ (W m^{-2})	95.0	102.0
$L^{\downarrow}$ (W m^{-2})	207.0	210.0
P (mm)	384.0	473.0
S (mm)	186.0	142.0
R (mm)	292.0	304.0

b. Discharge rates and snow course surveys

Runoff data are inferred from a water-level recorder located at 68.63°N, 149.40°W on the Upper Kuparuk River that operated throughout the spring melt period and summer of 1997. Although discharge rates are unavailable throughout the winter of 1996/97, they contribute only a small fraction of the total annual runoff as the snow cover and the frozen soil retain the water in temporary reservoirs. Table 2 indicates that runoff rates for the Upper Kuparuk for 1996–97 are of the order of 300 mm annually and that river discharge disposes 70% of the yearly precipitation input onto the basin, approaching the figure of 63% reported by McNamara et al. (1998) from 1993 to 1995.

Daily snow course measurements conducted at six sites during the spring transition period of 1997 within the Imnavait Creek watershed (located just to the northeast of the Upper Kuparuk River basin) provide the most comprehensive swe dataset closest to the study area. These data were collected as part of the ongoing field experiments in the region (Kane et al. 2000, 2002). The snow course surveys and the river discharge rates provide us with two independent datasets to validate the numerical simulations.

c. Digital elevation model

To derive topographic information required by the numerical models, a digital elevation model (DEM) of the Upper Kuparuk watershed has been acquired through the National Snow and Ice Data Center

(NSIDC; Walker 1996). The horizontal resolution of the DEM is 131 m. Although nearly 1 km in altitude separates the lowest and highest points in the watershed, more than 80% of the basin lies within ±250 m from its mean altitude of 967 m. From these data, the slope and aspect (defined here as the compass direction that a slope faces) for each grid point is evaluated and shows a predominance of east- and west-facing slopes (56% of all slopes) in the northward-flowing Upper Kuparuk River. As discussed in section 6b, the DEM is also used for distributed snowmelt simulations.

5. Numerical models

a. CLSM

The first model we use to simulate land surface processes in the Upper Kuparuk is the NSIPP CLSM (Koster et al. 2000; Ducharne et al. 2000). Although developed for application within the NSIPP GCM, the CLSM can also be operated ''offline,'' with the condition that an appropriate forcing dataset can be found to drive the model. In contrast to traditional land surface schemes, the CLSM employs the watershed as the fundamental hydrological unit instead of a rectangular grid cell. In each catchment unit, TOPMODEL (Beven and Kirkby 1979) equations are applied to relate the soil moisture distribution to topography. As such, the CLSM defines three soil moisture regimes in a single catchment, each with a distinct hydrological regime: a saturated zone, an unsaturated zone, and a wilting zone. The area occupied by each soil moisture regime is inferred from the distribution of the topographic index (tpi; Beven and Kirkby 1979). From the DEM, a discrete probability distribution function (pdf) of the tpi is computed. Following the methodology described by Koster et al. (2000) and Ducharne et al. (2000), a continuous gamma distribution is constructed to represent the pdf of tpi. The first three moments of this gamma distribution serve as input into the CLSM, and they are used to partition the catchment zones into a saturated (high tpi), unsaturated (intermediate tpi), and wilting (low tpi) areas. High values of tpi indicate areas with shallow slopes and large upstream areas (i.e., lowlands), and low values of tpi denote zones with large slopes and little upstream contributing areas (i.e., uplands). The CLSM includes a vegetation/canopy interception model that is based on the Mosaic LSM (Koster and Suarez 1996) and a permafrost dynamics model that determines the heat transfer and freeze/thaw cycle of the underlying ground (Stieglitz et al. 2001).

The CLSM is also coupled to a snow physics model that prognosticates the heat content, snow water equivalent, and snow depth for each of n snow layers, where n is typically set to 3 (Lynch-Stieglitz 1994; Stieglitz et al. 2001). This snow model considers most processes that lead to the formation and ablation of the snow cover, including precipitation, sublimation, snowmelt, compaction, liquid water infiltration, and refreezing. To insure a smooth transition between snow-free and snow-covered conditions, a minimum snow mass per unit area M_{min} of 13 kg m^{-2} is imposed on the snowpack. For values of snow mass $M_{\text{snow}} < 13$ kg m^{-2}, the fractional coverage of snow A_{snow} [0–1] over the whole watershed is given by

$$A_{\text{snow}} = \frac{M_{\text{snow}}}{M_{\text{min}}}. \tag{2}$$

Once $M_{\text{snow}} \geq M_{\text{min}}$, the catchment is considered to be entirely snow covered (i.e., $A_{\text{snow}} = 1$), and the snow cover is then allowed to grow vertically rather than horizontally. In this situation, however, the model assumes that the snow cover remains spatially uniform across individual catchments.

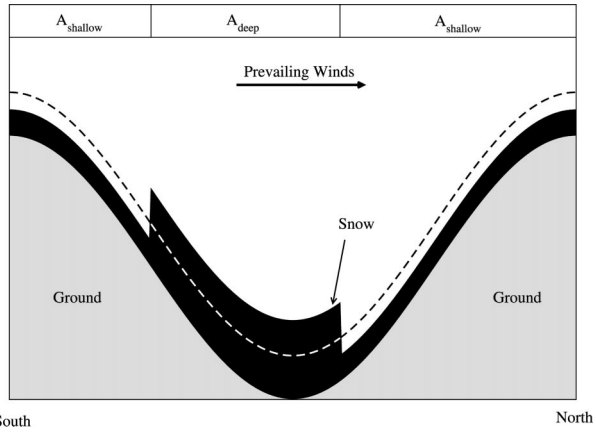

FIG. 3. The CLSM representation of the end-of-winter, nonuniform snow cover that arises because of wind redistribution of snow over the Upper Kuparuk River basin. Blowing snow carried by the prevailing southerly winds (here from left to right) is transported from erosion areas, leaving a shallow snow cover (of area A_{shallow}) at hilltops and windward slopes while mass accumulates in valleys and on lee slopes into a deep snow cover (of area A_{deep}). The basin mean swe, denoted by the dashed line, represents standard CLSM conditions with a uniform snow cover.

As clearly demonstrated in Fig. 1, however, the snow cover in the Upper Kuparuk basin displays considerable heterogeneity. In this region, snow is preferentially redistributed from windward slopes and hilltops onto lee slopes and lowland areas because of interactions between the prevailing winds, vegetation, and topography (Liston and Sturm 1998; Zhang et al. 2000). To include these effects into the CLSM, the following procedure is used: We first partition the snow cover into two areas, one with a shallow snow cover A_{shallow} representing erosion zones in the highlands and windward slopes, and another with a deep snow cover A_{deep} depicting accumulation zones in lowlands and on lee slopes (Fig. 3). The deep and shallow snow covers are modeled simultaneously in the CLSM by calling the snow scheme twice in succession, with each area imposed with the same meteorological forcing but evolving its own separate snow characteristics. To obtain the nonuniform

snow cover, however, snowfall is redistributed from the shallow to the deep snow cover, while conserving the total mass flux precipitating to the surface. Thus the precipitation falling onto the shallow and the deep snow cover is multiplied by a precipitation factor $p_{\text{shallow}}(\leq 1)$ and $p_{\text{deep}}(\geq 1)$ such that

$$A_{\text{shallow}}p_{\text{shallow}} + A_{\text{deep}}p_{\text{deep}} = 1, \quad (3)$$

as required by mass conservation principles. The precipitation factors are applied continuously during snowfall events in a CLSM simulation and control the amount of snow redistributed by wind. At each model time step, we then aggregate the output from the shallow and the deep snow cover according to their areal coverage. This methodology is reminiscent of the drift factors employed by Luce et al. (1998, 1999) to redistribute snowfall at Upper Sheep Creek, Idaho. The specification of these new free parameters is discussed in the appendix. During the ablation period, meltwater is transferred uniformly into the three soil catchment zones considered by the CLSM. This approach is used since the end-of-winter distribution of the deep and shallow snow cover with respect to the underlying saturated, unsaturated, and wilting zones, representing in an idealized fashion the lowland, intermediate, and upland regions in the catchment, respectively, is unknown. The relatively simple treatment of subgrid-scale snow heterogeneity by the CLSM compared to other models keeps the computational requirements of the simulations at acceptable levels for regional and global climate studies.

b. TOPLATS

The second numerical model used in this study consists of the TOPLATS, which relies on a combination of TOPMODEL concepts to describe lateral water fluxes in the subsurface (Famiglietti and Wood 1994a,b) and a soil–vegetation–atmosphere transfer (SVAT) scheme to model water and energy balance processes within the near-surface soil column (Peters-Lidard et al. 1997). Contrary to the CLSM, TOPLATS applies TOPMODEL equations in a distributed fashion across a catchment and as such is more suited for small-scale process studies. As the resolution of a DEM that delineates a given watershed increases, the computational demands of TOPLATS also escalate. The model includes a variety of cold season and boreal processes including a snowmelt and accumulation algorithm, a frozen soil parameterization, a moss layer representation, a forest understory model, and a scheme for open water bodies (Pauwels and Wood 1999a,b). The snow model is based on a two-layer representation of the snow cover with a thin surface layer interacting with the atmosphere and a more substantial subsurface layer exchanging energy with the underlying ground. The frozen soil representation captures both the thermal and hydraulic impacts of soil freezing.

For this study, two key topographic effects are added in TOPLATS to capture some of the small-scale physical processes that promote or retard snowmelt. These are the impact of elevation on air temperatures and the sensitivity of solar radiation fluxes to topographic slope and aspect angle. This requires that the snow cover now be modeled in a distributed fashion by TOPLATS using the DEM described in section 4c. Also, an adiabatic lapse rate of 6°C km^{-1} is taken to modify ambient air temperatures with elevation. Given that the elevation ranges from 570 to 1490 m above sea level in the DEM for the Upper Kuparuk basin, a difference of 5.5°C exists at all times between the lowest and highest points in the watershed. Despite this range in altitude, however, the mean air temperature change for all pixels in the Upper Kuparuk is only −0.4°C. Hourly variations in solar altitude and azimuth angles are calculated following Gates (1980) and are combined with local aspect and slope values derived from the 131-m DEM to spatially disaggregate the hourly insolation measurements.

6. Results

a. CLSM simulations

Two sets of numerical experiments, one with (‘‘nonuniform snow cover’’) and one without (‘‘uniform snow cover’’) the subgrid-scale snow parameterization, are conducted with the CLSM. For the subgrid-scale snow parameterization, we assign A_{shallow} and A_{deep} to be $2/3A_{\text{snow}}$ and $1/3A_{\text{snow}}$, respectively. Furthermore, we prescribe $p_{\text{shallow}} = 0.25$ and $p_{\text{deep}} = 2.5$, thereby imposing 10 times more precipitation onto the deep snow cover. The sources of these parameter values and their physical basis are discussed in the appendix. In both experiments, the CLSM is initially spun up for 20 yr using 1996 observational data until steady states for the water and energy balances, especially for the deep soil layers, are achieved. The CLSM then repeats an integration for 1996 and continues until the end of 1997. Using a time step of 20 min, the integration requires only a few minutes of CPU time using a typical Sun Microsystems computer with a 200-MHz processor. Results for the 1997 snowmelt period are then extracted and are discussed below. Some graphics include results from the TOPLATS simulations that are discussed in section 6b and then compared to the CLSM results in section 6c.

The evolution of the simulated snow covers during 1997 in each of the two numerical experiments is shown in Fig. 4. This is compared to the daily value of swe averaged from six snow course surveys conducted at Imnavait Creek. On average over the entire Upper Kuparuk watershed, the growth of the snow cover in the numerical experiments is similar during its formation period, as both attain a mean of about 120-mm swe, matching closely the observations collected on 12 May. In response to enhanced incoming radiation and near-surface air temperatures that surpass 0°C between 25 and 29 May (Fig. 2), the snow cover collapses rapidly

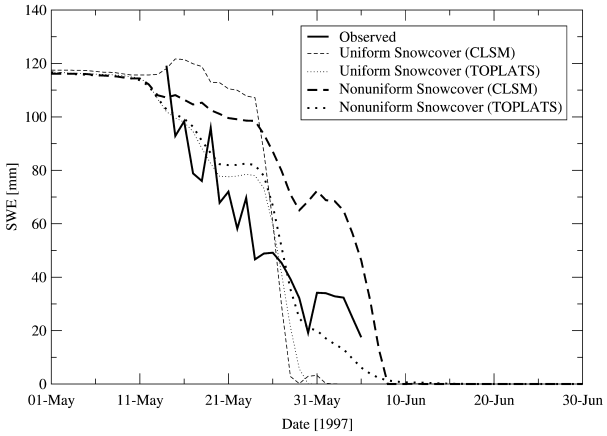

FIG. 4. Daily values of the observed swe compared to that simulated by the CLSM and TOPLATS, with a uniform and nonuniform snow cover for the Upper Kuparuk watershed from 1 May to 30 Jun 1997.

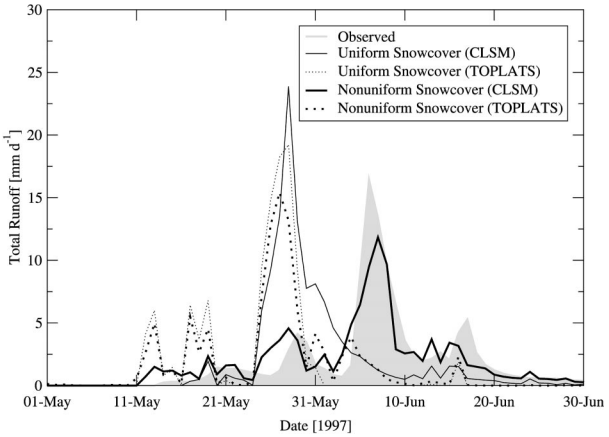

FIG. 5. Daily values of the observed runoff rates compared to those simulated by the CLSM and TOPLATS, with a uniform and a nonuniform snow cover for the Upper Kuparuk River from 1 May to 30 Jun 1997.

in the model with the uniform snow cover. In contrast, the nonuniform snow cover simulation displays a more gradual depletion of the snow cover that follows the observed trend. Snowmelt in late May is less intense than in the uniform snow cover experiment, retarding the complete ablation of the snow cover. Near-surface air temperatures again surpass the freezing point on 3 June, initiating the onset of further snowmelt. Note that a delay of a few days is apparent in the nonuniform snow simulation compared to observations; this may be attributed to the different topographic regimes (e.g., range of elevations) that exist in the Upper Kuparuk and Imnavait Creek basins.

Figure 5 depicts the temporal evolution of the observed daily streamflow of the Upper Kuparuk River versus that simulated by the CLSM during 1997. In the first experiment, the CLSM retains a uniform snow cover that melts rapidly and evenly across the Upper Kuparuk watershed. This leads to an early and intense peak in the simulated hydrograph as the CLSM model has difficulty representing the melt period. At this time, the simulated runoff rates attain 24 mm day^{-1} on 26 May, 50% larger than the 16 mm day^{-1} observed on 5 June, with a correlation coefficient of 0.10 between the two time series. Figure 5 reveals the improvement in the simulated runoff during the spring melt period when the subgrid-scale snow parameterization is incorporated into the CLSM. The correlation coefficient between the observed and simulated time series of river runoff has now improved to 0.88. By extending the ablation period by 9 days, the magnitude and the timing of the spring melt are now better captured by the model.

Given that snowmelt and a transition to a bare surface is accelerated over the basin area covered by a shallow snow cover, enhanced latent heat fluxes are expected in the CLSM nonuniform simulation. Figure 6 demonstrates that evaporative fluxes are indeed stronger in the nonuniform case between 23 and 27 May 1997 as the surface becomes partially bare and begins to warm up in response to solar radiation. However, the intensity of the evaporation is constrained at this time by relatively low air temperatures and high relative humidities (see Fig. 2). The complete disappearance of snow on 31 May 1997 in the uniform simulation yields a sudden increase in the corresponding latent heat fluxes. Once snowmelt has terminated in the nonuniform simulation, evaporative fluxes from the two simulations become identical, as evaporation remains atmospherically driven at this time.

Apart from the energy used as latent heat, other components of the surface energy balance are also affected by the presence of small-scale snow features. Figure 7a illustrates the changes in simulated total (or areally weighted) surface albedoes for the months of May and June 1997, with and without subgrid-scale snow in the CLSM. As discussed previously, the shallow snow cover simulated using the subgrid-scale snow scheme melts

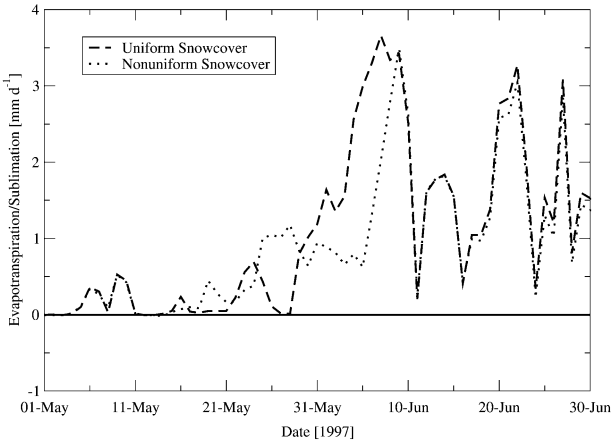

FIG. 6. Daily values of the evaporation fluxes simulated by the CLSM, with a uniform and nonuniform snow cover for the Upper Kuparuk watershed from 1 May to 30 Jun 1997.

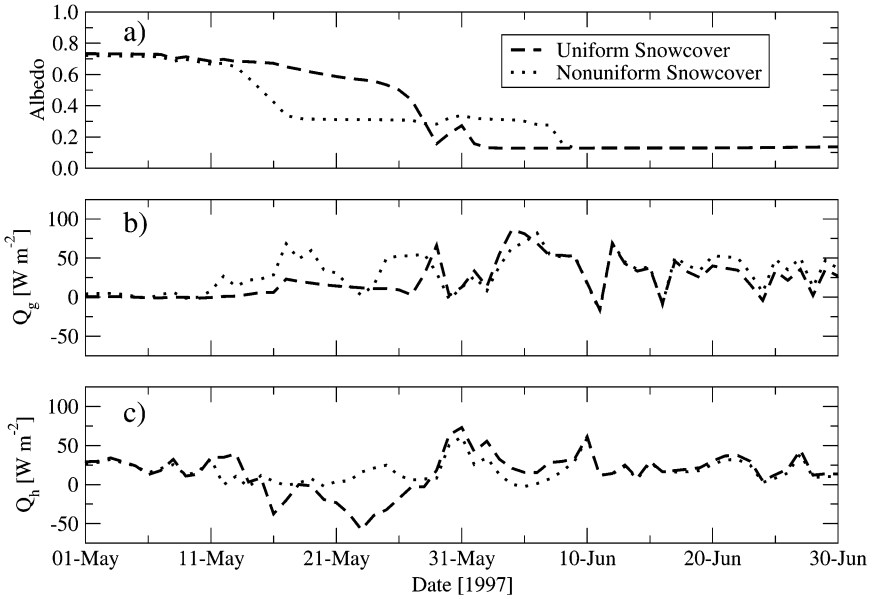

FIG. 7. Daily values of the (a) total surface albedo, (b) ground heat flux (Q_g; positive downward), and (c) sensible heat flux (Q_h; positive upward) simulated by the CLSM, with a uniform and nonuniform snow cover for the Upper Kuparuk watershed from 1 May to 30 Jun 1997.

about 10 days earlier than the uniform snow cover. This results in a sharp decrease in albedo during the first 2 weeks of May that is not otherwise observed with the previous version of the model. However, the persistence of some snowdrifts prevents the albedo from decreasing below 30% for another 20 days or so. An earlier decrease in albedo leads to a greater amount of solar radiation being absorbed by the surface that is consumed to heat the soil and the near-surface air. Thus, the ground and sensible heat fluxes are generally increased (Figs. 7b and 7c).

b. TOPLATS simulations

TOPLATS modeling is directed at assessing the impact of two key topographic features on the representation of snowmelt processes. Figure 8 describes the orography of the Upper Kuparuk watershed and the horizontal variability in corrected solar radiation fields due to the local aspect. Southward-facing slopes are subject to enhanced solar radiation because of their exposure to sunlight, whereas northward-facing slopes incur less incoming shortwave radiation. In addition, air temperatures from the forcing dataset were adjusted for each model grid point according to its elevation. Thus, regions of low (high) altitude experience enhanced (reduced) ambient air temperatures. The TOPLATS simulations are initiated on 30 April 1997 with the CLSM results shown in Fig. 4 of a mean 120-mm swe across the Upper Kuparuk watershed. It is assumed that the distribution (swe) and characteristics (cold content) are spatially uniform at this time. As with the CLSM, two TOPLATS simulations are conducted, one with (''nonuniform snow cover'') and one without (''uniform snow cover'') the effects of topography. TOPLATS is then integrated over a period of 60 days using a time step of 1 h. Wind redistribution of snow is not considered in this version of TOPLATS.

Figure 9 illustrates the impact of topography on the spatial patterns of snow retention (131-m resolution) predicted by TOPLATS at several times during the 1997 spring melt period. Observe the relatively quick melt of snow on the southwest-facing slope along the northeastern section of the Upper Kuparuk basin and the retention of snow on the north-facing slope along the southern edge of the watershed. In contrast, areas in the lee of mountains and at high elevations maintain a snow cover up to a month later than other regions of the Upper Kuparuk basin.

The time series of the observed and simulated swe for the spring of 1997 is illustrated in Fig. 4. Similar to the CLSM results, TOPLATS predicts a rapid collapse of the snow cover when spatially uniform conditions are assumed. In the nonuniform simulation, there is a delay in the complete melt of the snow cover. Thus, the effects of topography act to extend the melt period over a month, smoothing out the time series of swe. As in the CLSM simulation, the general evolution of snowcover conditions is well captured by TOPLATS.

The relationship between the spatial coverage of snow to the normalized mean basin swe, referred to here as a snow depletion curve, is shown in Fig. 10. Without topographic effects, snow coverage represented by TOPLATS is a delta function. As long as the swe is nonzero, the basin is considered to be entirely snow covered by the standard TOPLATS. When topographic effects

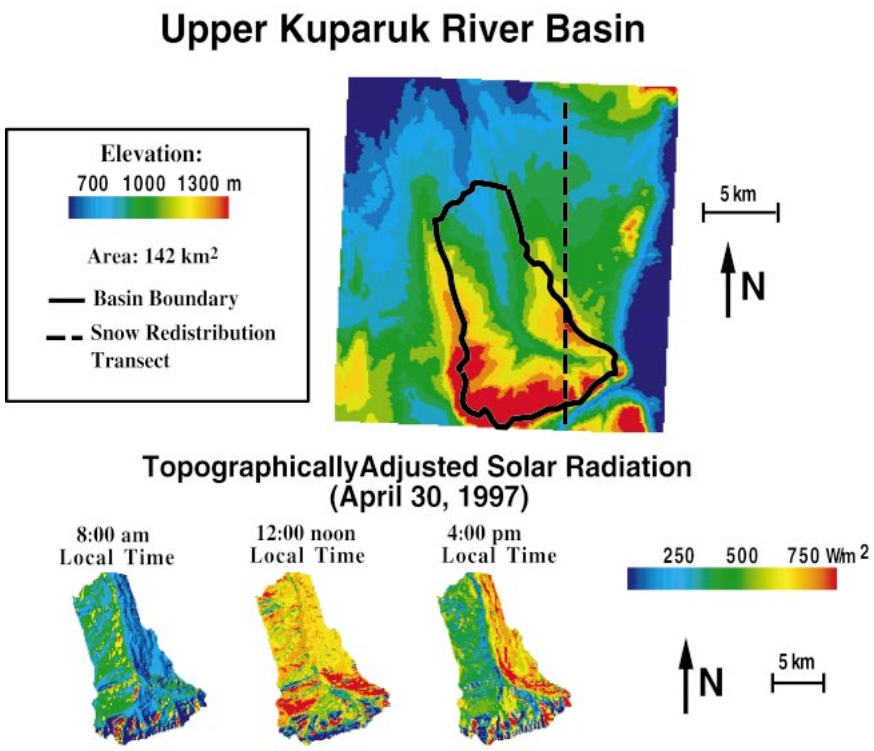

FIG. 8. Topographic map of the Upper Kuparuk watershed and the topographically adjusted solar radiation on 30 Apr 1997.

are introduced in the model, a gradual transition between the fully covered basin to a bare surface then appears. In two additional TOPLATS simulations, it is determined that slope and aspect, and not elevation, are the dominant topographic factors contributing to snowmelt heterogeneity in the Upper Kuparuk basin (not shown).

Daily values of the observed and simulated total river discharge are presented in Fig. 5. In the uniform ex-

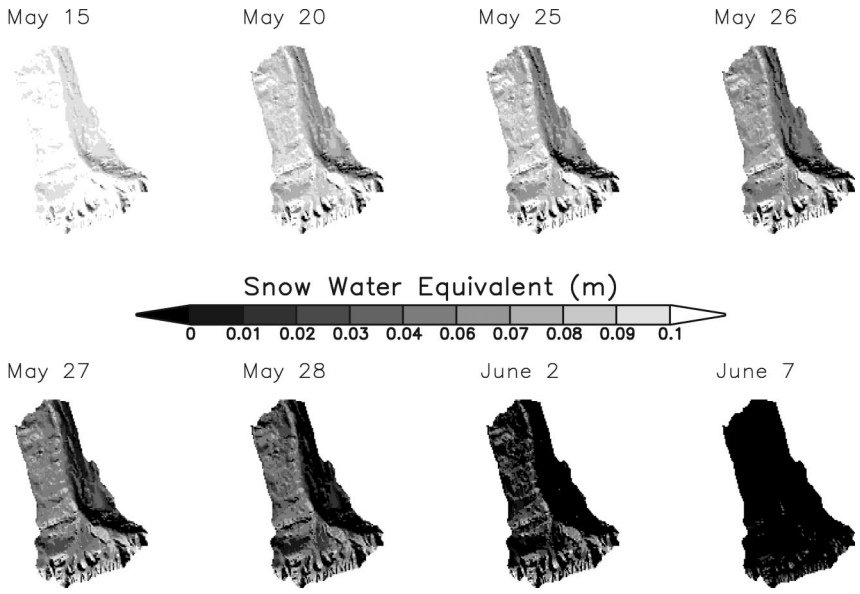

FIG. 9. The evolution of swe simulated by TOPLATS during the 1997 spring transition period in the Upper Kuparuk watershed, with topographically adjusted solar radiation and ambient air temperatures.

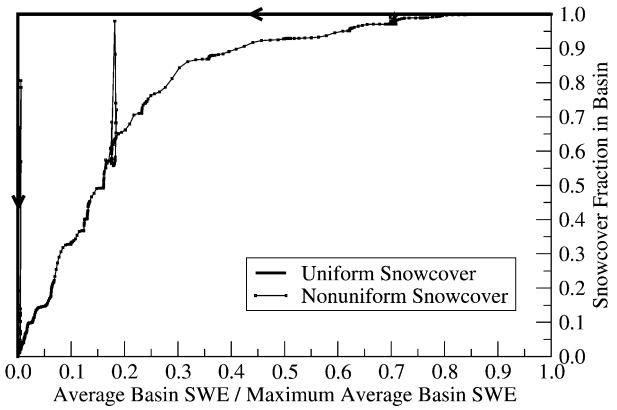

FIG. 10. The depletion curve of the normalized swe vs the snowcover areal fraction simulated by TOPLATS for the 1997 spring transition period of the Upper Kuparuk basin. Topography effects lead to a gradual decrease in both swe and area, whereas in the standard model, the snow cover ablates uniformly across the basin such that the depletion curve follows the direction of the arrows in this case.

periment, TOPLATS captures well the crest in river flow owing to meltwater. Similarly to the CLSM, however, the modeled peak precedes the observations by about 10 days. The inclusion of topographic effects diminishes slightly the simulated peak in river discharge rates without affecting its timing. Nevertheless, additional runoff during the first week of June arises from the inclusion of topography in the snowmelt simulation.

c. Intercomparison of simulation results

To better comprehend the effects of local- and small-scale snow heterogeneity on the numerical experiments, an intercomparison of CLSM and TOPLATS simulations is presented in this section. Figure 4 provides the temporal evolution of the observed swe and that simulated by the two models. This shows that with spatial homogeneity in snow-cover conditions, the two LSMs show a rapid collapse of swe during the spring transition period of 1997, with both models showing complete ablation of the snow cover by the end of May. In the nonuniform snow-cover experiments, on the other hand, the models disagree in the timing and in the rate of the snowmelt. Since there is greater disparity between the CLSM simulations with and without a uniform snow cover than in the corresponding TOPLATS experiments, the effects of snow redistribution by wind (represented by the CLSM subgrid-scale parameterization) play a larger role on the melt process than the effects of topography alone.

A similar conclusion can be achieved by close inspection of the observed and simulated discharge rates of the Upper Kuparuk River (Fig. 5). With a uniform snow cover, the peak river discharge rates simulated by the CLSM and TOPLATS precede the observations by 10 days. This delay vanishes when the subgrid-scale snow parameterization is included in the CLSM, whereas the corresponding TOPLATS simulation exhibits little change. From this intercomparison, we conclude that blowing snow affects spring discharge rates more so than variations in solar radiation owing to topographic effects. This also explains the inability of TOPLATS, even with a nonuniform snow cover owing to topographic effects, to accurately represent the timing of the spring discharge crest. Results in the following section discuss the potential for capturing wind redistribution effects in TOPLATS by combining it to a blowing snow model.

7. Concluding discussion

Snow-cover heterogeneity has been identified in this study as a key factor that requires special consideration in LSM simulations of the hydrologic regime of an Arctic watershed. To explore this issue we included, in varying degrees of complexity, snow-cover heterogeneity in two LSMs. The TOPLATS simulations employed a distributed approach to model snow-cover conditions during the spring melt period of 1997 in the Upper Kuparuk basin. In this set of experiments, the effects of elevation, slope, and aspect on snowmelt were modeled explicitly. By contrast, the CLSM simulations were designed to represent, using a simple parameterization, the effects of snow redistribution by wind on snow-cover conditions prior to and during the 1997 melt period. In the numerical simulations, the subgrid-scale variations in snow cover led to some significant changes in the predicted surface water and energy budgets of an Arctic watershed. These include 1) a delay and a reduction in the amplitude of the spring melt peak in water discharge, 2) changes in the intensity of evaporative fluxes, and 3) an enhancement of surface sensible and ground heat fluxes that arise from a reduction in total surface albedo. Given that up to 40% of the Northern Hemisphere is covered by seasonal snow cover (Hall 1988), added uncertainties in simulations of the regional or global climate may arise if such effects remain unresolved (Loth and Graf 1998; Lynch et al. 1998). This is especially true for a patchy snow cover since land–atmosphere interactions and feedbacks are tightly coupled during the spring transition period (Lynch et al. 1998; Liston 1999).

From the intercomparison of model results presented in section 6c, local and small-scale variations in snow-cover characteristics, including snow water equivalent and snow coverage, were shown to arise primarily from snow redistribution by wind, with secondary contributions owing to the topographic control of incoming solar radiation. To explore this finding in greater detail, we conducted two additional simulations of the snowmelt on a horizontal transect that is oriented along the prevailing wind direction. Both experiments were prescribed different initial conditions of snow, one with a uniform snow cover and another with a nonuniform snow cover owing to wind redistribution of snow (as

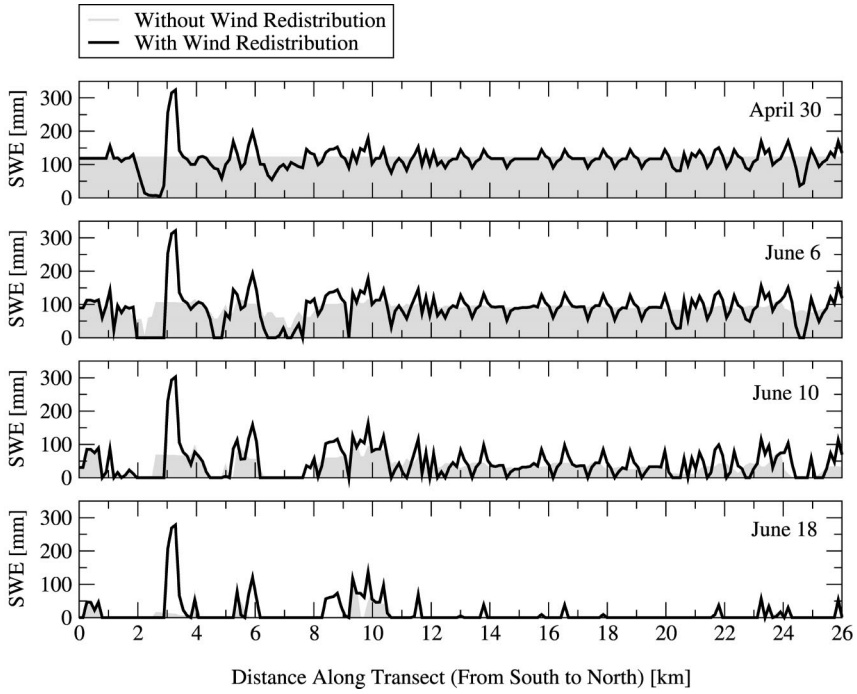

FIG. 11. The temporal evolution of swe along a south–north transect (shown in Fig. 8) in the Upper Kuparuk watershed during the 1997 spring transition period when wind redistribution, variations in air temperature, elevation and solar insolation as a function of slope, and aspect, are all considered in the TOPLATS simulation.

determined in the appendix). TOPLATS was then used to simulate snowmelt along this transect from 1 May to 30 June 1997, with the incoming solar radiation adjusted in both experiments according to local topographic effects.

Figure 11 demonstrates that snow persists over the transect, where it has accumulated into deep snowdrifts, until mid-June. Since the predominant winds are southerly, blowing snow generally enhances the effects of slope and aspect on snow retention during the spring melt of the Upper Kuparuk River basin. When only the effects of topography on incoming solar radiation are taken into account in the simulation, there is considerably less snow-cover heterogeneity at any one time than in the situation with wind redistribution. Since the deep snowdrifts arise on north-facing slopes, this implies that, for this particular case, the prescribed values of the new CLSM parameters represent the combined effects of slope, aspect, and wind redistribution on snow-cover evolution. The results from this supplemental experiment also confirm that blowing snow contributes more to snow-cover heterogeneity than the topographic effects on solar radiation in the Upper Kuparuk River basin.

Despite its simple formulation, the CLSM subgrid-scale snow-cover scheme has the caveat of introducing new free parameters that were calibrated to provide an improved representation of the hydrograph during the spring melt peak. Recall, for instance, that we prescribed $p_{\text{shallow}} = 0.25$ and $p_{\text{deep}} = 2.5$ (see the appendix). Despite this calibration, the new CLSM parameters can be constrained in several ways. For instance, the effects of elevation, slope, and aspect do not change from year to year (König and Sturm 1998). Thus, the TOPLATS experiments reveal the areas where melt is preferentially initiated each year as a result of topographic effects, irrespective of the amount of snow on the ground and of ambient atmospheric conditions. We would therefore expect the effects of orography to yield snow depletion curves with similar characteristics year after year. In addition to topographic effects, blowing snow events contribute to snow-cover heterogeneity in the Upper Kuparuk basin. Figures 12 and 13 demonstrate, however, that the annual frequency distributions of hourly wind speeds and directions vary only marginally at two field sites near the Upper Kuparuk basin over a period of 11 yr. At Toolik Lake, for instance, the observed winds are predominantly from the south-southeast (or 175°), accounting on average for 48% of wintertime wind directions. The narrow range between the minimum and maximum values in each wind speed and wind direction bin over the 11-yr record suggests that only minor interannual variations occur in the local wind regime. Therefore, snow-cover patterns in the Upper Kuparuk will incur preferential distributions according to the effects of both the local topography and climate. The recurring nature of these features thus suggests that the new CLSM subgrid-scale snow parameters are unlikely

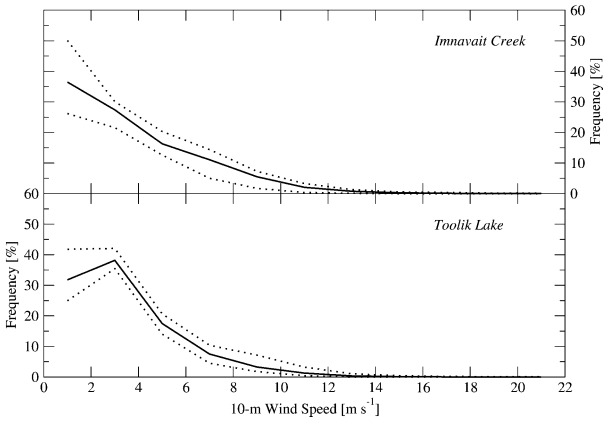

FIG. 12. The annual frequency distribution of hourly wind speeds for the period 1990–2000 at Imnavait Creek and Toolik Lake. The data exclude wind conditions during the warm season (Jun–Jul–Aug) of each year. The solid line depicts the 11-yr mean, while the dashed lines represent the range over that time period. There are data for 11 bins, each covering 2 m s^{-1}, beginning at 0–2 m s^{-1}.

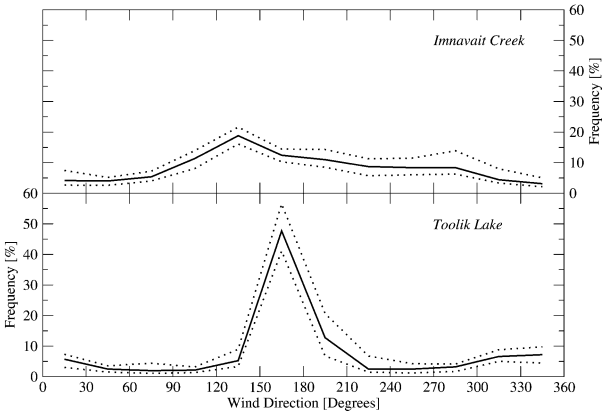

FIG. 13. The annual frequency distribution of hourly wind directions for the period 1990–2000 at Imnavait Creek and Toolik Lake. The data exclude wind conditions during the warm season (Jun–Jul–Aug) of each year. The solid line depicts the 11-yr mean, while the dashed lines represent the range over that time period. There are data for 12 bins, each covering 30°, beginning from 0°–30° for winds from the north-northeast, with a clockwise progression thereafter.

to change in time for this watershed. The quantification of the free parameters required by the simple CLSM subgrid-scale snow scheme can therefore be achieved using distributed snow and blowing snow models. Thus it is envisioned that the coupling of TOPLATS with the PIEKTUK model (Déry et al. 1998) would provide a robust, physically based approach to determine the combined effects of wind redistribution and topography on snowmelt.

In other regions of the Arctic, however, the interannual frequency and intensity of winter storms may vary more in response to changes in the large-scale environment, thus affecting significantly the amount of snow being redistributed (Liston 1999). In such cases, therefore, the assimilation of remote sensing data of snow in the numerical simulations is a consideration. The benefits of assimilating satellite-derived soil moisture data in regional and global climate models have already been established (e.g., Walker and Houser 2001; Crow and Wood 2002). Space-borne instruments are also now able to provide global snow-cover data at high spatial and temporal resolutions. For instance, the Moderate Resolution Imaging Spectroradiometer (MODIS) instruments mounted on NASA's *Terra* and *Aqua* satellites provide a suite of snow-cover data at various spatial and temporal scales (Hall et al. 2002). Parameterizations using the normalized difference snow index (NDSI) based on MODIS multispectral radiance data have also been developed to obtain subpixel ($<$500 m) values of the fractional snow coverage (Kaufman et al. 2002; Salomonson and Appel 2003). However, this approach does not provide the location covered by snow within a single grid cell, nor the swe contained in the snow cover. Since MODIS uses visible and infrared channels to detect the presence of snow, the persistence of low-level clouds in the Arctic during spring may also compromise its applicability. Other remote sensing data obtained from microwave channels, such as those from RADARSAT, provide snow-cover data at very high resolutions (10 m), but the interpretation of these measurements depends highly on snow characteristics such as snow density, temperature, and wetness content (Rango et al. 2000).

Apart from the generalization of the subgrid-scale parameterization using remote sensing data such as MODIS snow products, model development will focus on ways that variations in incoming solar radiation owing to topographic slope and aspect may be parameterized in the CLSM. Furthermore, an investigation of snow and ice damming and their impacts on river discharge during the spring transition period will be conducted (see the appendix). This will provide the necessary information to parameterize these effects in the CLSM and TOPLATS. Finally, the PIEKTUK blowing snow model will be upgraded to a 3D model and coupled to TOPLATS for a comprehensive modeling framework to study snow processes in a distributed fashion in Arctic watersheds.

Acknowledgments. This project has been funded through support from National Science Foundation Grants OPP-008236 (E. F. Wood) and OPP-0002369 (M. Stieglitz). Additional funding through the National Aeronautics and Space Administration's Seasonal-to-Interannual Prediction Project Grants NCC 5-510 and NAG 5-9759, through National Science Foundation Biocomplexity Grant ATM0221835, and through a National Science Foundation grant from the Division of Environmental Biology (Arctic LTER Project) to M. Stieglitz. The authors express their gratitude to R. D. Koster, S. Mahanama, M. J. Suarez (NASA GSFC), and J. W. Walker (University of Melbourne) for their support in the operation of the CLSM. We sincerely thank D.

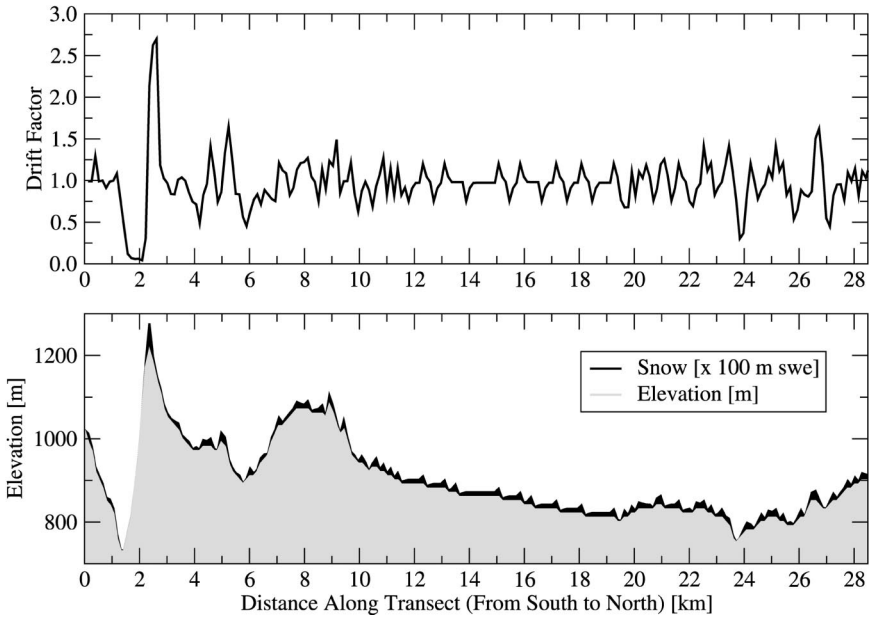

FIG. A1. The spatial distribution of elevation, as well as the end-of-winter snowdrift factor and swe predicted by the PIEKTUK blowing snow model, along a south–north transect (shown in Fig. 8) in the Upper Kuparuk basin during 1997.

L. Kane and L. D. Hinzman (University of Alaska, Fairbanks) for access to their comprehensive observational database for the North Slope of Alaska and J. Hobbie, G. R. Shaver, and J. M. Laundre (MBL, Woods Hole) for access to the Arctic LTER database. We are also grateful to Dr. G. W. Kling (University of Michigan) who provided us Fig. 1. Three anonymous reviewers and the editor (K. Mitchell) are thanked for their comments that helped strengthen the paper considerably.

APPENDIX

Derivation of Parameter Values for the CLSM Subgrid-Scale Snow Scheme

To establish the end-of-winter spatial distribution of snow in the Upper Kuparuk River basin, a distributed blowing snow model entitled PIEKTUK (Déry and Taylor 1996; Déry et al. 1998) is applied along a horizontal transect. The application of PIEKTUK then allows the derivation of the four bulk variables that are required by the CLSM subgrid-scale snow parameterization. PIEKTUK integrates in space four advection–diffusion equations (with source and sink terms included) to solve four prognostic variables: the mixing ratio q_b(kg kg^{-1}), total particle number concentration N(m^{-3}) of blowing snow, the air temperature T(K), and the water vapor mixing ratio q_v(kg kg^{-1}). The model activates only in circumstances when a ''blowing snow event'' is detected from the ambient conditions. Following Déry and Yau (1999b), this is defined as any time when the surface is snow covered, $T < 0$°C, and the wind speed U(m s^{-1}) surpasses a certain threshold, estimated following Li and Pomeroy (1997). The column-integrated snow mass transport rates (Q_t) are inferred from the vertical integration of the $q_b \times U$ profiles (Déry and Yau 1999a). Spatial variations in Q_t are associated with changes in the local wind speed. The wind speed profile varies according to step changes in surface characteristics of topographic slope and curvature (Liston and Sturm 1998). Computation of the divergence of Q_t along the horizontal transect then provides the snow mass that locally accumulates or erodes on the Arctic landscape.

PIEKTUK is integrated on a 1D transect (see Fig. 8 for its exact location) along the prevailing wind direction for the 1996/97 winter period forced by the observed meteorological dataset. Figure A1 illustrates the elevation along this transect, beginning from the south end of the Upper Kuparuk basin and moving toward the north. This simulation shows that the prevailing southerly winds preferentially erode snow form south-facing slopes and ridge tops to deposit the mass further downstream onto north-facing slopes and in valleys (Fig. A1).

Also shown in Fig. A1 are the end-of-winter snowdrift factors for 1996/97 inferred from the PIEKTUK simulation. The snowdrift factor is defined here as the local snow accumulation (swe) divided by the mean accumulation for the entire transect. Thus, values $>$ ($<$) 1 denote accumulation (erosion) areas (Luce et al. 1998). From the PIEKTUK simulation, we determine that 65% of the points along the transect are erosion (or deep snow cover) areas and the remaining 35% are accumulation (or shallow snow cover) areas. On average, about 2.2 times more swe is found in accumulation zones compared to erosion zones. After some tests with

the CLSM that include the subgrid-scale snow parameterization, we assigned $A_{\text{shallow}} = 2/3$ and $A_{\text{deep}} = 1/3$. This nearly matches the values inferred from the PIEKTUK simulation; however, we found it necessary to enhance the ratio of the deep to the shallow swe to 10 for an accurate representation of Upper Kuparuk River discharge rates. Thus the precipitation factors p_{shallow} and p_{deep} are assigned values of 0.25 and 2.5, respectively. The higher ratio of $p_{\text{deep}}/p_{\text{shallow}}$ required in the CLSM subgrid-scale snow parameterization indicates that the model is underrepresenting snow damming of meltwater and river ice, both physical processes that often delay and modify the intensity of discharge rates of high-latitude rivers during the spring transition period (Zhang et al. 2000; Prowse and Ferrick 2002). Recalibration of the parameters may be required once these processes are resolved by the CLSM.

REFERENCES

Anderson, E. A., 1973: National Weather Service River Forecast System—Snow Accumulation and Ablation Model. NOAA Tech. Memo. NWS Hydro-17, Silver Spring, MD, 217 pp.

Beven, K. J., and M. J. Kirkby, 1979: A physically-based variable contributing area model of basin hydrology. *Hydrol. Sci. Bull.*, **24,** 43–69.

Blöschl, G., R. Kirnbauer, and D. Gutknecht, 1991: Distributed snowmelt simulations in an apline catchment. 1. Model evaluation on the basis of snow cover pattern. *Water Resour. Res.,* **27,** 3171–3179.

Bowling, L. C., D. P. Lettenmaier, and B. V. Matheussen, 2000: Hydroclimatology of the Arctic Drainage Basin. *The Freshwater Budget of the Arctic Ocean,* E. L. Lewis et al., Eds., Nato Science Services, Vol. 2, Environmental Security, Vol. 7, Kluwer Academic, 57–90.

Cohen, J., and D. Rind, 1991: The effect of snow cover on the climate. *J. Climate,* **4,** 689–706.

Crow, W. T., and E. F. Wood, 2002: The value of coarse-scale soil moisture observations for regional surface energy balance modeling. *J. Hydrometeor.,* **3,** 467–482.

Déry, S. J., and P. A. Taylor, 1996: Some aspects of the interaction of blowing snow with the atmospheric boundary layer. *Hydrol. Proc.,* **10,** 1345–1358.

——, and M. K. Yau, 1999a: A bulk blowing snow model. *Bound.-Layer Meteor.,* **93,** 237–251.

——, and ——, 1999b: A climatology of adverse winter-type weather events. *J. Geophys. Res.,* **104,** 16 657–16 672.

——, and ——, 2001a: Simulation of an Arctic ground blizzard using a coupled blowing snow–atmosphere model. *J. Hydrometeor.,* **2,** 579–598.

——, and ——, 2001b: Simulation of blowing snow in the Canadian Arctic using a double-moment model. *Bound.-Layer Meteor.,* **99,** 297–316.

——, and M. Stieglitz, 2002: A note on surface humidity measurements in the cold Canadian environment. *Bound.-Layer Meteor.,* **102,** 471–479.

——, and M. K. Yau, 2002: Large-scale mass balance impacts of blowing snow and surface sublimation. *J. Geophys. Res.,* **107**, 4679, doi:10.1029/2001JD001251.

——, P. A. Taylor, and J. Xiao, 1998: The thermodynamic effects of sublimating, blowing snow in the atmospheric boundary layer. *Bound.-Layer Meteor.,* **89,** 251–283.

Ducharne, A., R. D. Koster, M. J. Suarez, M. Stieglitz, and P. Kumar, 2000: A catchment-based approach to modeling land surface processes in a general circulation model. 2. Parameter estimation and model demonstration. *J. Geophys. Res.,* **105,** 24 823–24 838.

Ellis, A. W., and D. J. Leathers, 1998: The effects of a discontinuous snow cover on lower atmospheric temperature and energy flux patterns. *Geophys. Res. Lett.,* **25,** 2161–2164.

Essery, R., L. Li, and J. Pomeroy, 1999: A distributed model of blowing snow over complex terrain. *Hydrol. Proc.,* **13,** 2423–2438.

Famiglietti, J. S., and E. F. Wood, 1994a: Multiscale modeling of spatially variable water and energy balance processes. *Water Resour. Res.,* **30,** 3061–3078.

——, and ——, 1994b: Application of multiscale water and energy balance models on a tallgrass prairie. *Water Resour. Res.,* **30,** 3079–3093.

Gates, D. M., 1980: *Biophysical Ecology*. Springer-Verlag, 635 pp.

Goodrich, L. E., 1982: The influence of snow cover on the ground thermal regime. *Can. Geotech. J.,* **24,** 421–432.

Hall, D. K., 1988: Assessment of polar climate change using satellite technology. *Rev. Geophys.,* **26,** 26–39.

——, G. A. Riggs, V. V. Salomonson, N. E. DiGirolamo, and K. J. Bayr, 2002: MODIS snow-cover products. *Remote Sens. Environ.,* **83,** 181–194.

Hartmann, M. D., J. S. Baron, R. B. Lammers, D. W. Cline, L. E. Band, G. E. Liston, and C. Tague, 1999: Simulations of snow distribution and hydrology in a mountain basin. *Water Resour. Res.,* **35,** 1587–1603.

Hinzman, L. D., and D. L. Kane, 1991: Snow hydrology of a headwater Arctic basin. 2. Conceptual analysis and computer modeling. *Water Resour. Res.,* **27,** 1111–1121.

——, and ——, 1992: Potential response of an Arctic watershed during a period of global warming. *J. Geophys. Res.,* **97,** 2811–2820.

——, ——, R. E. Gieck, and K. R. Everett, 1991: Hydrologic and thermal-properties of the active layer in the Alaskan Arctic. *Cold Reg. Sci. Technol.,* **19,** 95–110.

Jones, H. G., 1992: *Plants and Microclimate: A Quantitative Approach to Environmental Plant Physiology*. 2d ed. Cambridge University Press, 428 pp.

Kane, D. L., and L. D. Hinzman, cited 2002: Climate data from the North Slope Hydrology Research project. University of Alaska, Fairbanks, Water and Environmental Research Center, Fairbanks, AK. [Available online at http://www.uaf.edu/water/projects/NorthSlope/northslope.html.]

——, ——, C. S. Benson, and G. E. Liston, 1991: Snow hydrology of a headwater Arctic basin. 1. Physical measurements and process studies. *Water Resour. Res.,* **27,** 1099–1109.

——, ——, J. P. McNamara, Z. Zhang, and C. S. Benson, 2000: An overview of a nested watershed study in Arctic Alaska. *Nord. Hydrol.,* **31,** 245–266.

——, R. E. Gieck Jr., L. D. Hinzman, and E. K. Lilly, 2002: Meteorologic and hydrological data sets for the north slope of Alaska along the Kuparuk River watershed 1985–1997. Tech. Rep., Water Research Center, 52 pp. [Available from Water Research Center, Institute of Northern Engineering, University of Alaska, Fairbanks, Fairbanks, AK 99775-5860.]

Kaufman, Y. J., R. G. Kleidman, D. K. Hall, J. V. Martins, and J. S. Barton, 2002: Remote sensing of subpixel snow cover using 0.66 and 2.1 μm channels. *Geophys. Res. Lett.,* **29**, 1781, doi: 10.1029/2001GL013580.

König, M., and M. Sturm, 1998: Mapping snow distribution in the Alaskan Arctic using aerial photography and topographic relationships. *Water Resour. Res.,* **34,** 3471–3483.

Koster, R. D., and M. J. Suarez, 1996: Energy and water balance calculations in the Mosaic LSM. NASA Tech. Memo. 104606, Vol. 9, 59 pp.

——, ——, A. Ducharne, M. Stieglitz, and P. Kumar, 2000: A catchment-based approach to modeling land surface processes in a general circulation model. 1. Model structure. *J. Geophys. Res.,* **105,** 24 809–24 822.

Li, L., and J. W. Pomeroy, 1997: Estimates of threshold wind speeds for snow transport using meteorological data. *J. Appl. Meteor.,* **36,** 205–213.

Liston, G. E., 1999: Interrelationships among snow distribution, snowmelt, and snow cover depletion: Implications for atmospheric, hydrologic, and ecologic modeling. *J. Appl. Meteor.*, **38,** 1474–1487.

——, and M. Sturm, 1998: A snow-transport model for complex terrain. *J. Glaciol.,* **44,** 498–516.

——, and ——, 2002: Winter precipitation patterns in Arctic Alaska determined from a blowing snow model and snow-depth observations. *J. Hydrometeor.*, **3,** 646–659.

Loth, B., and H.-F. Graf, 1998: Modeling the snow cover in climate studies. 2. The sensitivity to internal snow parameters and interface processes. *J. Geophys. Res.,* **103,** 11 329–11 340.

Luce, C. H., D. G. Tarboton, and K. R. Cooley, 1998: The influence of the spatial distribution of snow on basin-averaged snowmelt. *Hydrol. Proc.,* **12,** 1671–1683.

——, ——, and ——, 1999: Sub-grid parameterization of snow distribution for an energy and mass balance snow cover model. *Hydrol. Proc.,* **13,** 1921–1933.

Lynch, A. H., D. L. McGinnis, and D. A. Bailey, 1998: Snow–albedo feedback and the spring transition in a regional climate system model: Influence of land surface model. *J. Geophys. Res.,* **103,** 29 037–29 049.

Lynch-Stieglitz, M., 1994: The development and validation of a simple snow model for the GISS GCM. *J. Climate,* **7,** 1842–1855.

McKay, G. A., and D. M. Gray, 1981: The distribution of snowcover. *Handbook of Snow,* D. M. Gray and D. H. Male, Eds., Pergamon Press, 153–190.

McNamara, J. P., D. L. Kane, and L. D. Hinzman, 1998: An analysis of streamflow hydrology in the Kuparuk River Basin, Arctic Alaska: A nested watershed approach. *J. Hydrol.,* **206,** 39–57.

Osterkamp, T. E., and M. W. Payne, 1981: Estimates of permafrost thickness from well logs in northern Alaska. *Cold Reg. Sci. Technol.,* **5,** 13–27.

——, and V. E. Romanovsky, 1996: Characteristics of changing permafrost temperatures in the Alaskan Arctic, U.S.A. *Arct. Alp. Res.,* **28,** 267–273.

Pauwels, V. R. N., and E. F. Wood, 1999a: A soil–vegetation–atmosphere transfer scheme for the modeling of water and energy balance processes in high latitudes. 1. Model improvements. *J. Geophys. Res.,* **104,** 27 811–27 822.

——, and ——, 1999b: A soil–vegetation–atmosphere transfer scheme for the modeling of water and energy balance processes in high latitudes. 2. Application and validation. *J. Geophys. Res.,* **104,** 27 823–27 839.

Peters-Lidard, C. D., M. S. Zion, and E. F. Wood, 1997: A soil–vegetation–atmosphere transfer scheme for modeling spatially variable water and energy balance processes. *J. Geophys. Res.,* **102,** 4303–4324.

Pomeroy, J. W., and D. M. Gray, 1995: Snowcover accumulation, relocation and management. NHRI Science Rep. 7, Saskatoon, SK, Canada, 144 pp.

Prasad, R., D. G. Tarboton, G. E. Liston, C. H. Luce, and M. S. Seyfried, 2001: Testing a blowing snow model against distributed snow measurements at Upper Sheep Creek, Idaho, United States of America. *Water Resour. Res.,* **37,** 1341–1350.

Prowse, T. D., and M. G. Ferrick, 2002: Hydrology of ice covered rivers and lakes: Scoping the subject. *Hydrol. Proc.,* **16,** 759–762.

Rango, A., A. E. Walker, and B. E. Goodison, 2000: Role of snow and ice. *Remote Sensing in Hydrology and Water Management,* G. A. Schultz and E. Engman, Eds., Springer, 239–270.

Roesch, A., M. Wild, H. Gilgen, and A. Ohmura, 2001: A new snow cover fraction parameterization for the ECHAM4 GCM. *Climate Dyn.,* **17,** 933–946.

Salomonson, V. V., and I. Appel, 2003: Estimating fractional snow cover from MODIS using the normalized difference snow index (NDSI). *Remote Sens. Environ.,* in press.

Slater, A. G., and Coauthors, 2001: The representation of snow in land surface schemes: Results from PILPS 2(d). *J. Hydrometeor.,* **2,** 7–25.

Stewart, R. E., K. K. Szeto, R. F. Reinking, S. A. Clough, and S. P. Ballard, 1998: Midlatitude cyclonic cloud systems and their features affecting large scales and climate. *Rev. Geophys.,* **36,** 245–273.

Stieglitz, M., J. Hobbie, A. Giblin, and G. Kling, 1999: Hydrologic modeling of an Arctic tundra watershed: Toward pan-Arctic predictions. *J. Geophys. Res.,* **104,** 27 507–27 518.

——, A. Giblin, J. Hobbie, M. Williams, and G. Kling, 2000: Simulating the effects of climate change and climate variability on carbon dynamics in Arctic tundra. *Global Biogeochem. Cycles,* **14,** 1123–1136.

——, A. Ducharne, R. Koster, and M. Suarez, 2001: The impact of detailed snow physics on the simulation of snow cover and subsurface thermodynamics at continental scales. *J. Hydrometeor.,* **2,** 228–242.

——, S. J. Déry, V. E. Romanovsky, and T. E. Osterkamp, 2003a: The role of snow cover in the warming of Arctic permafrost. *Geophys. Res. Lett.,* **30**, 1721, doi:10.1029/2003GL017337.

——, J. Shaman, J. McNamara, G. W. Kling, V. Engel, and J. Shanley, 2003b: An approach to understanding hydrologic connectivity on the hillslope and the implications for nutrient transport. *Global Biogeochem. Cycles,* in press.

Walker, D. A., cited 1996: GIS data from the Alaska North Slope. National Snow and Ice Data Center. [Available online at http://arcss.colorado.edu/data/arcss017.html.]

——, and M. D. Walker, 1996: Terrain and vegetation of the Imnavait Creek watershed. *Landscape Function and Disturbance in Arctic Tundra,* J. F. Reynolds and J. D. Tenhunen, Eds., Ecological Studies, Vol. 120, Springer-Verlag, 73–108.

Walker, J. P., and P. R. Houser, 2001: A methodology for initializing soil moisture in a global climate model: Assimilation of near-surface soil moisture observations. *J. Geophys. Res.,* **106,** 11 761–11 774.

Walland, D. J., and I. Simmonds, 1996: Sub-grid-scale topography and the simulation of Northern Hemisphere snow cover. *Int. J. Climatol.,* **16,** 961–982.

Winstral, A., K. Elder, and R. E. Davis, 2002: Spatial snow modeling of wind-redistributed snow using terrain-based parameters. *J. Hydrometeor.*, **3,** 524–538.

Woo, M.-K., and P. Marsh, 1978: Analysis of error in the determination of snow storage for a small high arctic basin. *J. Appl. Meteor.,* **17,** 1537–1541.

——, and P. Steer, 1986: Monte Carlo simulation of snow depth in a forest. *Water Resour. Res.,* **22,** 864–868.

Xiao, J., R. Bintanja, S. J. Déry, G. Mann, and P. A. Taylor, 2000: An intercomparison among four models of blowing snow. *Bound.-Layer Meteor.,* **97,** 109–135.

Yang, D., and Coauthors, 2000: An evaluation of the Wyoming gauge system for snowfall measurement. *Water Resour. Res.,* **36,** 2665–2677.

Zhang, T., T. E. Osterkamp, and K. Stamnes, 1996: Some characteristics of the climate in Northern Alaska, U.S.A. *Arct. Alp. Res.,* **28,** 509–518.

Zhang, Z., D. L. Kane, and L. D. Hinzman, 2000: Development and application of a spatially-distributed Arctic hydrological and thermal process model (ARHYTHM). *Hydrol. Proc.,* **14,** 1017–1044.